Available online at www.sciencedirect.com

ScienceDirect

Physics Procedia 83 (2016) 104 – 113

Physics Procedia

9th International Conference on Photonic Technologies - LANE 2016

Selective ablation of thin nickel-chromium-alloy films using ultrashort pulsed laser

Linda Pabst[a,]*, Robby Ebert[a], Horst Exner[a]

[a]*Hochschule Mittweida, Tecikumplatz 17, 09648 Mittweida, Germany*

Abstract

The selective ablation of 100 nm thin Nickel-Chromium-alloy films on glass substrate was investigated using femtosecond laser pulses (λ=1030 nm, τ_p=170 fs, $E_{p,max}$=7 µJ). The influence of the processing parameters such as fluence, pulse number and pulse repetition rate on the ablation process was examined. Single and multiple pulses ablation thresholds of the Nickel-Chromium-alloy film were determined and the incubation coefficient calculated. Optical and electron microscopy were employed to characterize the patterned area. As a result, different irradiation morphologies were observed, dependent from the processing parameters. A processing window for film side ablation of the Nickel-Chromium-alloy film without damaging the underlying glass substrate was found, however, the edge of the ablation craters were covered with laser induced periodic surface structures (LIPSS).

Peer-review under responsibility of the Bayerisches Laserzentrum GmbH

Keywords: thin film processing; rear-side ablatio; front side ablation; damage morphology characteristics; ultrashort pulse laser

1. Introduction

Nickel-Chromium-Alloy films have some interesting properties which makes them an ideal material in various fields of engineering. In electronic and electrical manufacturing NiCr is used as embedded thin film resistor (ETFR) and replaces semiconducting resistors for GaAs monolithic microwave integrated circuits (MMICs). Furthermore, it is used as direct load or potentiometers in hybrid circuits. For these applications NiCr was chosen because of its high reliability, high electrical resistivity, good power dissipation and small temperature coefficient of resistance.

* Corresponding author. Tel.: +49-3727-976-335 ; fax: +49-3727-976343 .
E-mail address: pabst@hs-mittweida.de

Peer-review under responsibility of the Bayerisches Laserzentrum GmbH
doi:10.1016/j.phpro.2016.08.019

Furthermore, NiCr has a very good wear and corrosion resistance, therefore, it is used as fusible links in read only memories. Due to the low temperature dependence of the gauge factor, NiCr has also applications for stain gauge. (Kazi et al. (2003), Kazi et al. (2006), Vinayak et al. (2006), Vinayak et al. (2007), Danisman et al. (2010))

Therefore, the deposition of Nickel-Chromium thin films on various materials has been thoroughly investigated in the last decades. As deposition method mostly vapour deposition and sputtering were discussed. The influence of the material composition and the deposition parameters on the film resistivity and the temperature coefficient of resistance were examined. (Swanson et al. (1967), Kazi et al. (2006), Lai et al. (2013), Danisman et al. (2010))

To produce these devices the thin film need to be party ablated to generate the desired functionality. Besides lithography laser structuring is a promising tool for selective structuring of thin films. Laser structuring is, for example, already commercially applied for serial interconnection of CIGS (Copper-Indium-Gallium-Diselenide) thin film solar cells. (Compaan et al. (2000))

Several studies of laser processing of metallic Chromium (Heise et al. (2012), Wang et al. (2010), Kim et al. (2007)) and Nickel (Preuss et al. (1994), Güdde et al. (1998)) thin films were performed. However, as far as the authors know, no detailed study of selective laser structuring of Nickel-Chromium-Alloy films was performed.

Therefore, the present work focuses on fundamental investigations on the selective laser structuring of a thin Nickel-Chromium alloy film on glass substrate using ultra-short pulsed laser radiation. The influence of the processing parameters such as fluence, pulse number and pulse repetition rate on the ablation process was investigated. The observed irradiation morphologies were described and corresponding threshold values determined.

2. Materials and Experimental setup

2.1. Experimental setup

For the experiments a femtosecond laser (Clark MXR Impulse™) was used. The laser emitted laser pulses at a central wavelength of 1030 nm and linear polarisation. The laser operated at a pulse repetition rate of 1.024 MHz and provided a pulse width of approximately 170 fs. The pulse repetition rate could be changed without influencing other laser parameters using a pulse picker. With this device, the pulse repetition rate f_p could be divided by an integer n down to f_p/n. The pulse picker selected only every n^{th} pulse and blocks the others. If not otherwise mentioned, the repetition rate was set to 32 kHz. The maximum pulse energy was 7 µJ. The pulse energy could be precisely controlled using an attenuator consisting of an AOM (acousto optical modulator). The laser beam was focused at normal incidence onto the sample surface by the use of an 80 mm objective, resulting in a focal radius of approximately 24.4 µm. The sample was mounted on a positioning stage allowing the precise positioning of the sample in the focal plane. All experiments were performed in air environment at normal incidence. The produced surface structures were analyzed with an optical microscope and a Scanning Electron Microscope (SEM).

2.2. Material

The experiments were carried out on a 100 nm thin Nickel-Chromium-alloy film. The chemical composition of the layer was measured using an EDX (energy dispersive X-ray spectroscopy). The alloy consisted of approximately 56 atom percent Nickel, 42 atom percent Chromium and 2 atom percent Tin, as well as traces of Aluminum and Iron. Thus, it was a Nickel base alloy with a high proportion of Chromium. Float glass was used as substrate with a thickness of 2.5 mm.

2.3. Experimental procedure

First, investigations of single and multiple pulses irradiation from the film side were performed. For this purpose, the sample was irradiated with increasing pulse energy and different pulse numbers. After laser irradiation the sample was investigated using an optical microscope and Scanning Electron Microscope (SEM) to analyze the morphology changes as well as the size of the ablation area. In order to get accurate measurements the dimensions of at least five irradiation spots were measured for each parameter set. This allowed the calculation of the average

value and a corresponding standard deviation was evaluated. Due to the imperfect Gaussian beam profile of the laser spot, the ablation area was measured and a corresponding equivalence diameter was determined. Furthermore, the single and multiple pulses ablation thresholds were calculated. The influence of the processing parameters such as fluence, pulse number and pulse repetition rate on the ablation process was investigated.

3. Results and Discussion

3.1. Ablation morphologies

In Fig. 1 selected, characteristic morphologies observed after single and multiple pulses irradiation from the film side are shown. Single pulse irradiation only led to a modification or partly ablation of the thin film. At low fluences a melt rim appeared around the irradiation area, see Fig. 1 (q), but no significant ablation of the film was attained. This morphology was referred to as heat affected zone (HAZ). At mediate fluences different morphology transitions were observed (k,g), mainly visible in optical microscope images due to color changes. Only at high fluences a partly ablation of the film, in the center part of the irradiation area, was achieved (a).

The morphology transitions after irradiation with two pulses at low fluence were similar to the morphology changes after single pulse irradiation, see Fig. 1 (r,l). By increasing the fluence a partly ablation of the film was obtained in the center of the irradiation area (l). At higher fluences the surface of the layer melted and appeared smooth (h). By increasing the fluence the complete film was melted down to the substrate. Even at the highest possible fluence melt residuum remained inside the ablation area (b). With five or more pulses the irradiation area was covered with periodic structures. These structures were aligned perpendicular to the incident electric field vector of the laser beam and had a period of approximately the wavelength of the laser, (i-l, m,n). Therefore, these structures were Laser Induced Periodic Surface Structures (LIPSS) and had similar characteristics like Low Spatial Frequency LIPSS (LSFL) reported in the literature (Bonse et al. (2010), Duft et al. (2009), Straub et al. (2012)).
LIPSS are normally reported by laser processing of bulk materials. (Bonse et al. (2010), Duft et al. (2009), Straub et al. (2012), Bashir et al. (2012)) The appearance of LIPSS on thin films is only rarely investigated (Zamfirescu et al. (2009), Scoricati et al. (2012), Pabst et al. (2015)). Most commonly two types of LIPSS are reported after irradiation of surfaces with linear polarized laser beams. The Low Spatial Frequency LIPSS (LSFL) have a period of approximately equal to the wavelength of the laser and are aligned perpendicular or for large band gab materials parallel to the electric field vector of the laser. The High Spatial Frequency LIPSS (HSFL) have a period significant smaller than the wavelength of the laser. The appearance of the LIPSS is dependent form the processing parameters and the type of material which is irradiated. (Bonse et al. (2010), Duft et al. (2009), Straub et al. (2012), Pabst et al. 2015)) Up to now the fundamental mechanism for the generation of LIPSS is not completely understood and various theories of the generation are still subject of controversial discussion. Widely accepted models include the interference of a surface scattered wave with the incident laser beam (Emmony et al. (1973)), the excitation of Surface Plasmon Polaritons (Bashir et al. (2012), Straub et al. (2012)), the second harmonic generation (Duft et al. (2009)) and self-organisation processes (Costache et al. (2003), Varlamova et al. (2006)).

With ten and more pulses, at high fluences, the complete film was ablated in the irradiation center without any residuum (d-f). However, the edge quality was poor, due to the LIPSS which still remained at the outer part of the irradiation area. This was on the basis of the lower fluence on the rim of the ablation area caused by the Gaussian beam profile. At high pulse numbers and low fluences another type of LIPSS appeared on the thin film (p,v), which was aligned parallel to the polarization direction and had a higher period and therefore could be associated with coarse LIPSS. In the literature the coarse LIPSS are reported to appear in the center of the irradiation area at higher fluences interrupting the appearance of the LSFL. This morphology has a higher period up to 6 µm and is aligned parallel to the polarization direction of the electric field vector of the laser. (Guan et al. (2013), Bonse et al. (2010), Costace et al. (2003)) These structures are sometimes described in the literature as coarse ripple (Costache et al. (2003)), micro-ripple (Guan et al. (2013)) or grooves (Bonse et al. (2010)).

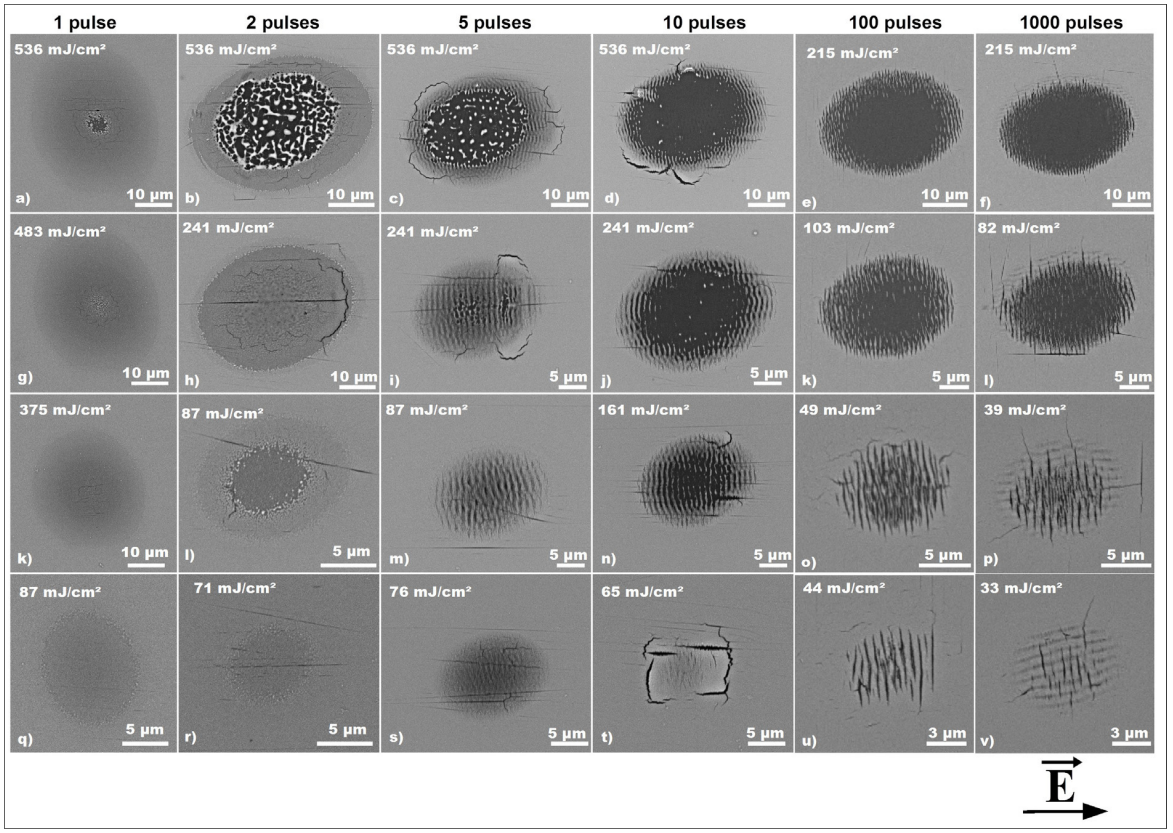

Fig. 1. SEM images of ablation morphologies after single and multiple pulse irradiation by film side irradiation.

With high pulse numbers and high fluences the surface of the glass substrate was also covered with LIPSS. This type of LIPSS was also aligned perpendicular to the polarization direction, however, the period was significant smaller than the wavelength. With that these structures had similar characteristics then HSFL reported in literature (Bonse et al. (2010), Pabst et al. (2015), Duft et al. (2009)).

3.2. Single and multiple pulse ablation thresholds

By applying a pulse energy above the damage threshold (E_{th}) a damage area with a diameter D_{eff} can be observed. For a Gaussian beam profile the dependence between the damage area and the applied pulse energy can be described by equation (1), relating $(D_{eff})^2$ to $Ln(E_p)$. By extrapolating the linear regression fit to the x-axis ($D_{eff}=0$), the damage threshold (E_{th}) can be obtained. Furthermore, the beam dimension (radius) (w_{86}) can be calculated from the slope. (Liu (1982)) The threshold fluence was then calculated by equation (2) using the spot size $w_{86} = 24.4$ µm, calculated from the raw beam diameter and the focal length of the focussing objective. The value for the spot size was confirmed by a beam profile measurement in the focal plane.

$$D_{eff}^2 = 2 \cdot w_{86} \cdot \ln\left(\frac{E_p}{E_{th}}\right) \tag{1}$$

$$F_{\max} = \frac{2 \cdot E_p}{\pi \cdot w_{86}^2} \tag{2}$$

Fig. 2 (a) and (b) show the semi-logarithmic plot of the squared measured dimension as a function of the applied pulse energy for the heat affected zone (HAZ) and the complete ablation of the thin film for different pulse numbers, respectively. Furthermore, the standard deviations of the measured data and of the regression curve are given. The film modification or heat affected zone (HAZ) was defined as the area where the microstructure of the film was visible changed during the laser irradiation process without complete ablation of the thin film. A nearly linear dependence in the semi-logarithmic plot was observed for the film ablation (b) and the curves were shifted towards lower pulse energies at higher applied pulse numbers. The curves for the modification diameters laid all close to each other, however, they showed a bend at a pulse energy of 1 µJ, fluence of 107 mJ/cm². Therefore, the low and high pulse energy region were analysed separately. From the ablation curve the ablation thresholds and spot sizes were evaluated and are shown in Fig. 3 (a) and (c), respectively, as a function of the applied pulse number. The calculated spot sizes from the slope were lower than the applied spot size and were independent from the applied pulse numbers, see Fig. 3 (c), only a slight difference to the single pulse irradiation was observed. Furthermore, different spot sizes were evaluated in the high and low pulse energy regime (compare blue and red), indicating the bend in the regression curve. The calculated spot sizes were similar for the complete ablation and the HAZ in the low pulse energy regime (green and red). The deviation between the spot size calculated from the raw beam diameter and from the regression curve might be due to the non-perfect Gaussian beam profile used in the experiments, because equation (1) is only valid for a perfect Gaussian beam profile.

The pulse number had no significant influence on the threshold fluences for the heat affected zone, see Fig. 3 (a, blue and red). However, for the ablation a reduction of the threshold fluence was observed with increasing pulse number (green triangle). The single pulse threshold for modification of the thin Nickel-Chromium-alloy film were 42.1 ± 2.7 mJ/cm² and 64.7 ± 6.5 mJ/cm² for the low and high pulse energy regime, respectively. With single pulses a complete ablation of the thin film was not achieved.

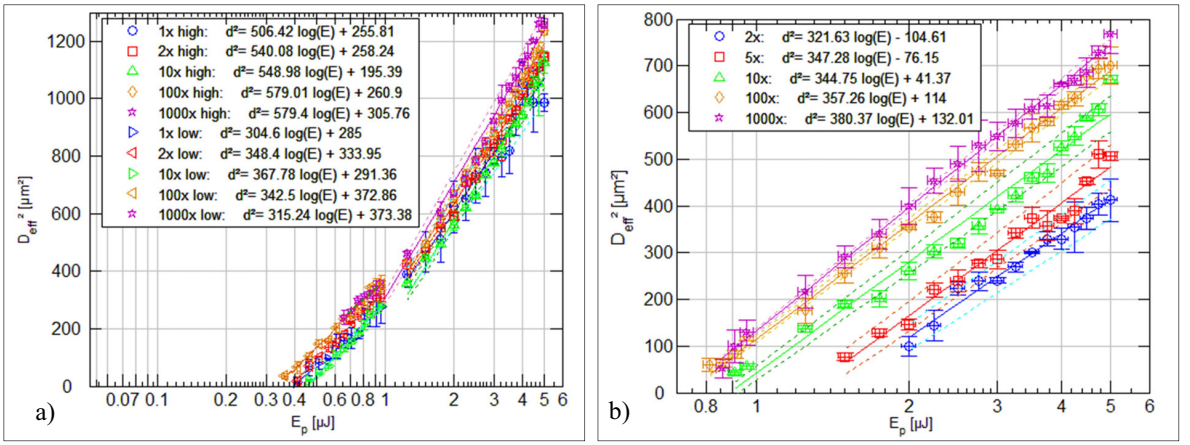

Fig. 2. squared ablation diameters as a function of the applied pulse energy for various applied pulse numbers (a) for the heat affected zone and (b) for the compleate ablation of the film.

The multiple pulses ablation threshold $F_{th}(N)$ for N applied laser pulses is related to the single pulse ablation threshold $F_{th}(1)$ by the incubation model introduced by Jee et al. (1988), see equation (3). Thereby, S is the incubation coefficient and characterizes the extent to which incubation occurs. The smaller the incubation coefficient the stronger is the incubation effect.

$$F_{th}(N) = F_{th}(1) \cdot N^{S-1} \tag{3}$$

Up to now the physical mechanism responsible for the reduction of the ablation threshold with increasing pulse number is not completely understood and various theories are still subject of controversial discussion. (Di Niso et al. (2014), Byskov-nielsen et al. (2010), Gallais et al. (2014)) Each laser pulse modifies the initial surface and therefore changes the surface properties. This influences the absorption of the material and the ablation threshold. The local material transition changes due to the first laser pulses may be caused by surface defects (Scorticati et al. (2012)), surface oxidation (Jaeggi et al. (2011), Bonse et al. (2000)) or increased surface roughness (Scorticati et al. (2012), Jaeggi et al. (2011), Byskov-Nielson et al. (2010)). As a consequence the surface reflectivity decreases and the energy absorption into the material increases. (Scorticati et al. (2012), Jaeggi et al. (2011)) Furthermore, plastic deformation resulting from laser induced stress field (Jee et al. (1988), Monnion et al. (2004)) or surface oxidation (Bonse et al. (2000)) can store energy in the material. These mechanisms may decrease the ablation threshold.

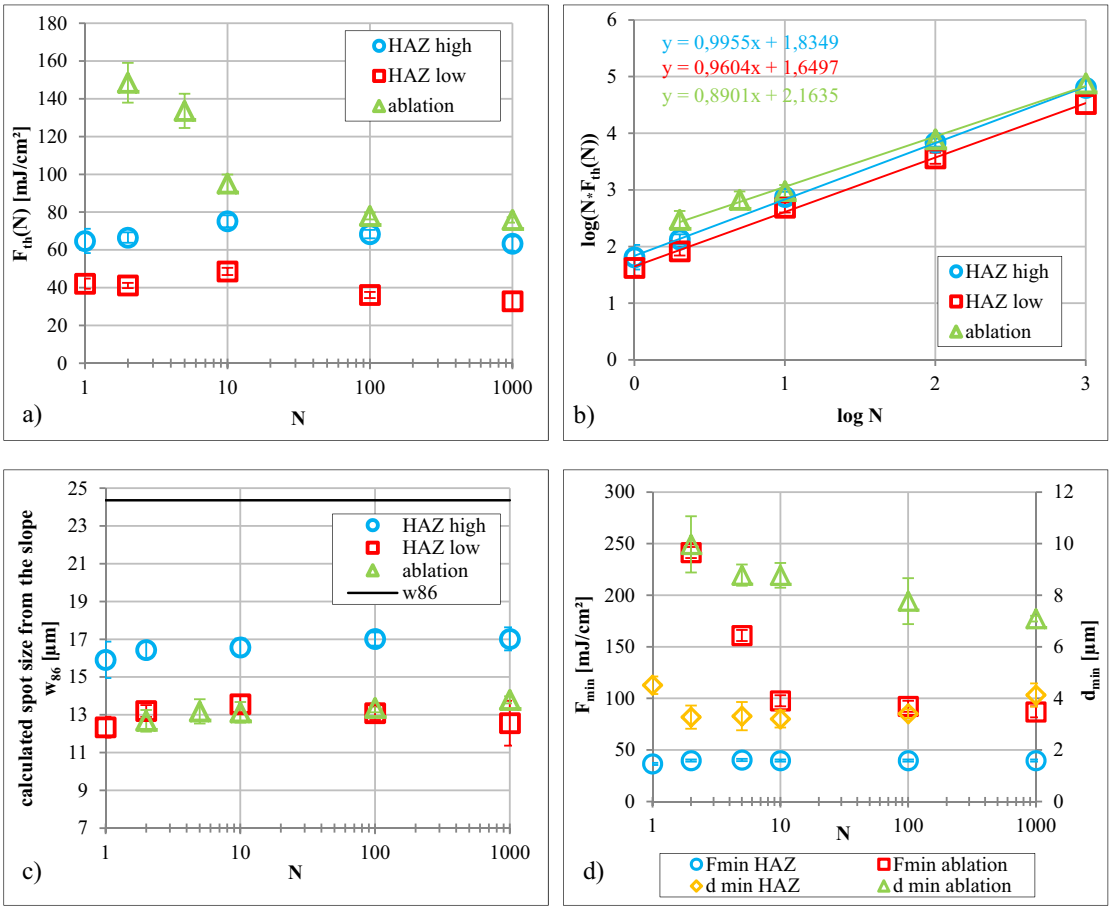

Fig. 3. (a) multiple pulse ablation thresholds calculated from the curves given in Fig. 2, (b) accumulated threshold fluences, (c) calculated spot sizes from the slope of the curves from Fig. 2 and (d) minmal measured morphology diameters and the minimal fluence for these morphologies all as a function of the applied pulse number.

In Fig. 3 (b) logarithmic plots of the accumulated fluence ($N_{*}F_{th}(N)$) as a function of the applied pulse number N are shown. From the logarithmic plot a linear dependence were obtained. The fit yielded an incubation coefficient S of 0.96 ± 0.02 and 0.89 ± 0.03 for the heat affected zone and the complete ablation of the Nickel-Chromium-Alloy film, respectively. The value of the incubation coefficient indicated an accumulation behaviour for the complete ablation of the film with increasing pulse number. The heat affected zone, however, showed no significant incubation behaviour. The different behaviour of the layer might be explained by the different processes for generating the morphologies. For the HAZ only a modification without significant ablation of the layer occurred, whereas the complete ablation was achieved due to melting and evaporation of the thin film. Furthermore, the single pulse thresholds were estimated from the regression curve with 145.7 ± 12.8 mJ/cm², 44.6 ± 1.3 mJ/cm² and 68.4 ± 4.6 mJ/cm² for the complete ablation of the thin film, the low and high pulse energy regime of the film modification, respectively. These values were in good agreement with the modification threshold of single pulse irradiation. However, with single pulse irradiation a fully ablation of the thin film was not achieved, even at much higher fluences of 536 mJ/cm², well above the calculated ablation threshold of 145.7 ± 12.8 mJ/cm².
The minimal modification diameters for different morphologies were measured, dependent from the applied pulse number, see Fig. 3 (d). The minimal diameters of the heat affected area were approximately 4 µm (yellow rhombus) independent from the applied pulse number. However, the minimal ablation diameters decreased with increasing pulse number (green triangle) from approximately 10 µm to 7 µm. Thereby, much smaller modification (HAZ) and ablation diameters were generated compared to the applied spot diameter of 48.8 µm. The generated structures were by a factor of 12 and 5 smaller than the spot diameter for the modification and the ablation, respectively. The applied fluences for the minimal ablation diameters decreased with increasing pulse number (red square) from 240 mJ/cm² to 87 mJ/cm². Whereas the applied fluences for the minimal heat affected area were independent from the pulse number with 39 ± 1.4 mJ/cm². These values were in good agreement with the calculated threshold fluences, see Fig. 3 (a).

3.3. Influence of the pulse repetition rate

Furthermore, the influence of the pulse repetition rate on the ablation results was investigated using 100 pulses per ablation spot, see Fig. 4. The repetition rate could be decreased without influencing other laser parameters due to the use of the pulse picker. At high pulse repetition rates a lager ablation crater was observed at the same fluences compared to low repetition rates, see Fig. 4 (a-e and f-j). This can be explained by a heat accumulation due to the poor thermal conductivity of the glass substrate. At high repetition rates an accumulation of heat, due to the short time between the subsequent pulses, can result in local rise of the temperature (Gallais et al. (2014), Di Niso et al. (2014)). A cracking of the glass substrate as well as the thin film occurred, see Fig. 4 (a-c). Due to the high repetition rate the thermal load in the glass substrate was too high and led to the cracking. Furthermore, at high repetition rates, especially at 1024 kHz, the edge of the ablation crater was blurred, possible due to a higher amount of melting (a,f,k,p). With decreasing pulse repetition rate LIPSS were better pronounced (f-j). At pulse repetition rates of 205 kHz and below no significant difference in the ablation morphology was observed. Therefore, the applicable repetition rate was limited to a maximum of 205 kHz. With decreasing pulse repetition rate the minimal ablation fluence increased, see (p-t). By applying a significant number of laser pulses, especially at high pulse repetition rates, a heat accumulation can occur, due to the short time interval between the subsequent laser pulses. This leads to a local rise in the temperature generating better absorption probability and therefore a reduction of the ablation threshold. (Gallais et al. (2014), Di Niso et al. (2014))

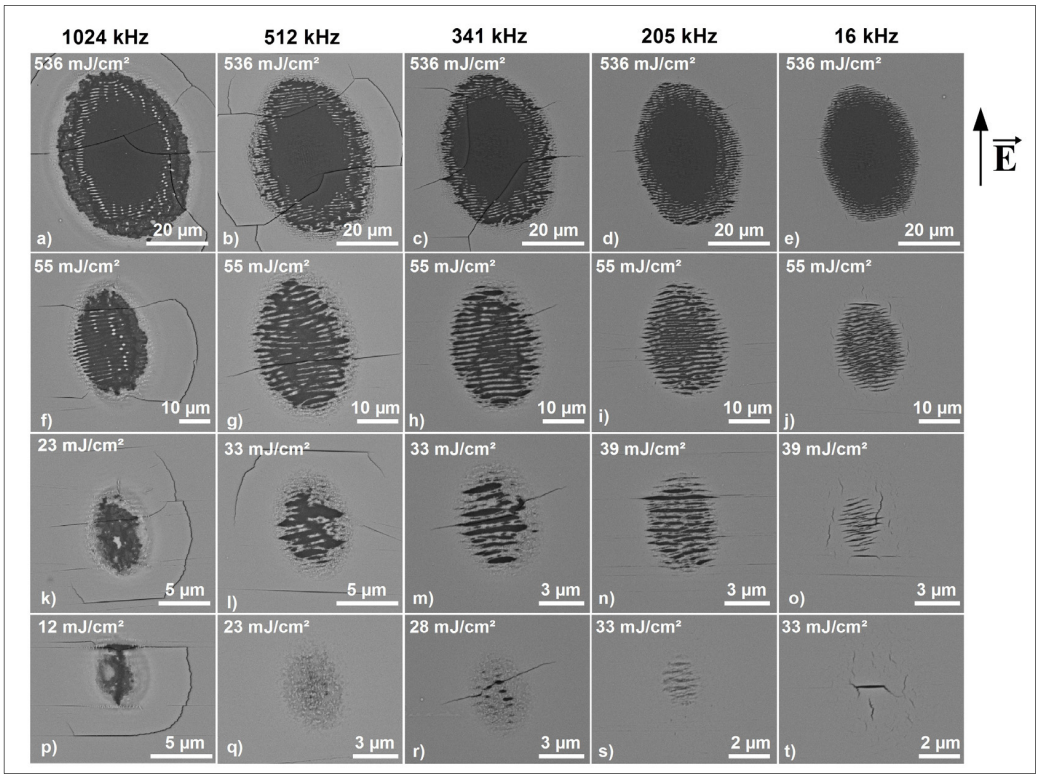

Fig. 4. SEM images of ablation morphologies at various pulse repetition rates with 100 pulses per area by front side irradiation.

In Fig. 5 (a) the squared diameters of the HAZ, measured at the outer part of each irradiation crater, as a function of the applied pulse energy for different pulse repetition rates are shown. Each ablation curve showed again a bend at a pulse energy of 1 µJ, fluence of 107 mJ/cm². Therefore, the low and high pulse energy region were analysed separately. From the ablation curves the ablation threshold as well as the spot size were calculated and are represented in Fig. 5 (b). The ablation threshold decreased significant with increasing pulse repetition rate in the low fluence regime (light blue circles) and slightly in the high fluence regime (green triangles). A rapid decrease of the threshold fluence with increasing pulse repetition rate was reported by Tan et al. (2009) for 300 nm gold films on a silicon substrate using repetition rates up to 13 MHz. The authors calculated the heat accumulation in the thin gold film using the one-dimensional heat conduction equation. The calculations showed no significant heat accumulation in the thin gold film, which could explain the reduction of the threshold fluence with increasing pulse repetition rate. (Tan et al. (2009)) However, the simulations of Weber et al. (2014) indicated a significant heat accumulation in CrNi-steel even at pulse repetition rates well below 1 MHz. The heat accumulation seems to depend strongly on the material parameters.

Furthermore, the minimum fluences at which a modification of the thin film was achieved were determined (black circles). These minimal fluences also decreased with increasing pulse repetition rate and were in good agreement with the calculated threshold fluences (light blue circle). For the low fluence regime the calculated spot sizes remained nearly constant at approximately 13.7 µm (red squares), whereas in the high fluence regime the calculated spot sizes increased with increasing pulse repetition rate (yellow rhombus) from 17.1 to 21.6 µm for 16 to 1024 kHz, respectively. With increasing pulse energy the influence on the heat accumulation increased, especially at higher pulse repetition rates, resulting in a higher extension of the HAZ. Therefore, the slope of the ablation curves were steeper and a higher spot size could be calculated at higher pulse repetition rates. An increase of the accumulated heat with increasing pulse repetition rate as well as with increasing pulse energy was simulated by Weber at al. (2014). The minimal ablation diameters, dependent from the pulse repetition rate were measured (purple cross) and also remained nearly constant at 4.8 µm, well below the applied spot diameter of 48.8 µm.

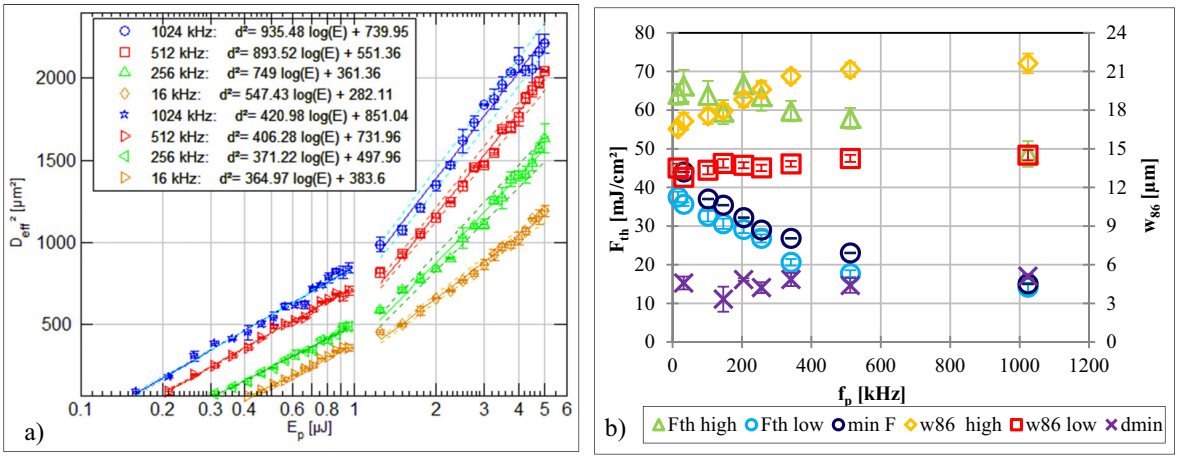

Fig. 5. (a) squared diameter of HAZ as a function of the applied pulse energy for different pulse repetition rates and (b) determined threshold fluences and spot sizes as well as the minimal measured ablation diameter and minimal fluence for these ablations as a function of the pulse repetition rate for 100 applied pulses.

4. Summary

Selective structuring of 100 nm thin Nickel-Chromium alloy films on glass substrate was investigated using femtosecond laser pulses. The influence of processing parameters such as fluence, pulse number and pulse repetition rate were investigated.

The ablation process was characterized by melting. By applying multiple pulses different ablation morphologies were observed. With single pulse irradiation only a modification or partly ablation of the thin film was achieved. At higher pulse numbers the film was completely removed without damaging the underlying glass substrate. However, at the edge of the ablation crater, an area covered by Laser Induced Periodic Surface Structures (LIPSS) was observed. At high pulse numbers and high fluences also the surface of the glass substrate was covered with LIPSS, however, at all investigated processing parameters the glass substrate was not ablated. The modification threshold of the Nickel-Chromium-alloy film was found to be 42.1 ± 2.7 mJ/cm² and the incubation factor was evaluated of 0.96 ± 0.02 and 0.89 ± 0.03 for modification and melting of the thin film, respectively.

Furthermore, an influence of the pulse repetition rate on the ablation process was found. The ablation threshold decreased with increasing repetition rate indicating an accumulation effect at high pulse repetition rates. Due to heat accumulation in the glass substrate at higher pulse repetition rates, a cracking of the glass occurred. Therefore, a maximal usable pulse repetition rate of 205 kHz was found.

Acknowledgements

The authors thank the European Social Fund (ESF) for funding the Project ULTRALAS No. 8231016.

References

Kazi, I.H., Wild, P.M., Moore, T.N., Sayer, M., 2003. The electrical behavior of nicrome (80/20 wt.%) film. Thin Solid Films 433, 337-343.

Kazi, I.H., Wild, P.M., Moore, T.N., Sayer, M., 2006. Characterisation of sputtered nicrome (Ni-Cr 80/20 wt.%) films for strain gauge applications. Thin Solid Films 515, 2602-2606.

Danisman, M., Canseverm N., 2010. Effect of Cr content on mechanical and electrical properties of Ni-Cr thin films. Journal of Alloys and Compounds 493, 649-653.

Vinayak, S., Vyas, H.P., Vankar, V.D., 2007. Microstructure and electrical characteristics of Ni-Cr thin films. Thin Solid Films 515, 7109-7116

Vinayak, S., Vyas, H.P., Muraleebharan, K., Vankar, V.D., 2006. Ni-Cr thin film resistor fabrication for GaAs monolithic microwave integrated circuits. Thin Solid Films 514, 52-57.

Lai, L., Fu, X., Sun, R., Du, R., 2013. Comparison of microstructure and electrical properties of NiCr alloy thin film deposited on different substrates. Surface & Coatings Technology 235, 552-560.

Swanson, J.G., Campbell, D.S., 1967. The structural and electrical properties of 80:20 NiCr thin films. Thin Solid Films 1, 183-202.

Compaan, A.D., Matulionis, I., Nakade, S., 2000. Laser scribing of polycrystalline thin film. Optics and Lasers in Engineering 34, 15-45.

Kim, J., Na, S., 2007. Metal thin film ablation with femtosecond pulsed laser. Optics & Laser Technology 39, 1443-1448.

Güdde, J., Hohlfeld, J., Müller, J.G., Matthias, E., 1998. Damage threshold dependence on electron-phonon coupling in Au and Ni films. Applied Surface Science 127-129, 40-45.

Preuss, S., Matthias, E., Stuke, M., 1994. Sub-picosecond UV-laser ablation of Ni films. Applied Physics A 59, 79-82.

Wang, W., Jiang, G., Mai, X., Wang, Shao, J., Yang, C., 2010. Damage mechanism and morphology characteristics of chromium film in femtosecond laser rear-side ablation. Applied Surface Science 256, 3612-3617.

Heise, G., Domke, M., Konrad, J., Sarrach, S., Sotrop, J., Huber, H.P., 2012. Laser lift-off initiated by direct induced ablation of different metal thin films with ultra-short laser pulses. Journal of Physics D: Applied Physics 45, 315303.

Liu, J., 1982. Simple technique for measurements of pulsed Gaussian-beam spot sizes. Optical Letters 7 (Issue 5), 196-198.

Jee, Y., Becker, M. F., Waler, M., 1988. Laser-induced damage on single-crystal metal surfaces. Journal of the Optical Society of America B 5 (Issue 3), 648-659.

Di Niso, F., Caudiuso, C., et al., 2014. Role of heat accumulation on the incubation effect in multi-shot laser ablation of stainless steel at high repetition rates. Optics Express 22, 1220-12210.

Mannion, P.T., Magee, J., et al. 2004. The effect of damage accumulation behavior on the ablation thresholds and damage morphology in ultrafast laser micro-machining of common metals in air. Applied Surface Science 233, 275-287.

Bashir, S., Rafique, M. S., Husinsky, W. 2012. Femtosecond laser-induced subwavelength ripples on Al, Si, CaF2 and CR-39. Physics Research B 275, 1-6.

Costache, F., Henyk, M., Reif, J. 2003. Surface patterning on insulators upon femtosecond laser ablation. Appl. Surf. Science 208-209, 486-491.

Straub, M., Afshar, M., et al. 2012. Surface plasmon polariton model of high-spatial frequency laser-induced periodic surface structure generation in silicon. Journal of Applied Physics 111, 124315.

Duft, D., Rosenfeld, A., et al. 2009. Femtosecond laser-induced periodic surface structures revisited: A comparative study on ZnO. Journal of Applied Physics 105, 034908.

Varlamova, O., Costache, F., et al. 2006. Self-organized pattern formation upon femtosecond laser ablation by circularly polarized light. Applied Surface Science 252, 4702-4706.

Bonse, J., Krüger, J., 2010. Pulse number dependence of laser-induced periodic surface structures for femtosecond laser irradiation of silicon. Journal of Applied Physics 108, 034903.

Bonse, J., Sturm, H., Schmidt, D., Kautek, W., 2000. Chemical, morphological and accumulation phenomena in ultrashort-pulse laser ablation of TiNi in air. Applied Physics A 71, 657-665.

Guan, Y.C.; Zhou, W.; et al. 2013. Femtosecond laser-induced iridescent effect on AZ31B magnesium alloy surface. Journal of Physics D: Applied Physics 46.

Tan, B.; Venkatakrishnan, K. 2006. A femtosecond laser-induced periodical surface structure on crystalline silicon. Journal of Micromechanics and Microengineering 16, 1080-1085.

Tan, B., Dalili, A. Venkatakrishnan, K., 2009. High repetition rate femtosecond laser nano-machining of thin films. Appl. Physics A 95, 537-545.

Emmony, D.C.; Howson, R.P.; Willis, L.J. 1973. Laser mirror damage in germanium at 10.6 µm. Applied Physics Letter 23, Issue 11, 598-600.

Pabst, L., Perrie, W., et al. 2015. Femtosecond Laser Induced Periodic Surface Structures of ITO thin films on glass substrate. Scientific Reports, Journal of the University of Applied Sciences Mittweida 4/2015, 158-162.

Zamfirescu, M., Ulmeanu, M., et al., 2009 Femtosecond Laser Induced Periodic Surface Structures on ZnO Thin Films. JLMN-Journal of Laser Micro/Nanoengineering 4, 7-10.

Byskov-Nielsen, J., Savolainen, J.M., et al., 2010. Ultra-short pulse laser ablation of metals: threshold fluence, incubation coefficient and ablazion rates. Applied Physics A 101, 97-101.

Scorticati, D., Römer, G., et al., 2012. Ultra-short-pulsed laser-machined nanogratings of laser-induced periodic surface structures on thin molybdenum layer. Jounal of Nanophotonics 6, 063528, 1-11.

Jaeggi, B., Neuenschwander, B., et al., 2011. Influence of the Pulse Duration in the ps-Regime on the Ablation Efficiency of Metals. Physics Procedia 12, 164-171.

Gallais, L., Bergeret, E., et al., 2014. Ultrafast laser ablation of metal films on flexible substrates. Applied Physics A 115, 177-188.

Weber, R., Graf, T., et al., 2014. Heat accumulation during pulsed laser materials processing. Optical Society of America 22, 11312-11324.